Droplet dissolution driven by emerging thermal gradients and Marangoni flow

Binglin Zeng (曾炳霖) ◉,[1,2,3] Yuliang Wang (王玉亮) ◉,[2,4,*] Christian Diddens ◉,[1]
Harold J. W. Zandvliet ◉,[3,†] and Detlef Lohse ◉[1,5,‡]

[1]*Physics of Fluids Group and Max Planck Center for Complex Fluid Dynamics, J. M. Burgers Centre for Fluid Dynamics, University of Twente, P.O. Box 217, 7500 AE Enschede, The Netherlands*
[2]*School of Mechanical Engineering and Automation, Beihang University, 37 Xueyuan Road, Haidian District, Beijing 100191, China*
[3]*Physics of Interfaces and Nanomaterials, MESA + Institute, University of Twente, P.O. Box 217, 7500 AE Enschede, The Netherlands*
[4]*Ningbo Institute of Technology, Beihang University, Ningbo 315832, China*
[5]*Max Planck Institute for Dynamics and Self-Organization, Am Fassberg 17, 37077 Göttingen, Germany*

The lifetime τ of an isothermal and purely diffusively dissolving droplet in a host liquid scales as $\tau \sim R_0^2$ with its initial radius R_0 [Langmuir, Phys. Rev. **12**, 368 (1918)]. For a droplet dissolving due to natural convection driven by density differences, its lifetime scales as $\tau \sim R_0^{5/4}$ [Dietrich *et al.*, J. Fluid Mech. **794**, 45 (2016)]. In this paper we experimentally find and theoretically derive yet another droplet dissolution behavior, resulting in $\tau \sim R_0^4$. It occurs when the dissolution dynamics is controlled by local heating of the liquid, leading to a modified solubility and a thermal Marangoni flow around the droplet. The thermal gradient is achieved by plasmonic heating of a gold nanoparticle decorated sample surface, on which a sessile water droplet immersed in water-saturated 1-butanol solution is sitting. The resulting off-wall thermal Marangoni flow and the temperature dependence of the solubility determine the droplet dissolution rate, resulting in a shrinkage $R(t) \sim (\tau - t)^{1/4}$ of the droplet radius and thus in $\tau \sim R_0^4$.

I. INTRODUCTION

Droplet dissolution in another liquid is a process of utmost importance in process technology. It is ubiquitous in a wide range of important applications, such as in the food and cosmetic industry [1], for drug delivery [2,3], in micro- and nanoextraction [4–6], microfabrication [7,8], autochemotaxis of droplets [9,10], etc.

On small scales, the droplet dissolution process is purely diffusive, controlled by the concentration gradient outside the droplet, normal to its surface. The process is mathematically equivalent to droplet evaporation in an ambient gas or bubble dissolution in an ambient liquid (see the review on nanodroplets and nanobubbles by Lohse and Zhang [11], prior reviews on droplet evaporation [12,13], or classical papers by Langmuir [14], Epstein and Plesset [15], Deegan [16], Popov [17], or in the context of evaporating aerosols, Wells [18]). For such droplets, when in thermal equilibrium with their surroundings, the radius R decreases in time with a square root behavior $R(t) \sim (\tau - t)^{1/2}$,

---

*wangyuliang@buaa.edu.cn
†h.j.w.zandvliet@utwente.nl
‡d.lohse@utwente.nl

implying that the lifetime τ of the droplet is quadratic with its initial radius, $\tau \sim R_0^2$, the so-called D^2 law, where "D" stands for the droplet diameter (twice the radius R_0).

For larger scales, however, natural convection can become important for the dissolution process. This holds for both bubbles [19] and droplets [20,21], and without an external flow, i.e., natural convection. The origin of the natural convection is a density difference emerging through the dissolution process (local depletion or enhancement of one heavier or lighter species), leading to buoyant forces, locally driving the natural convection and considerably enhancing the dissolution rate. Dietrich *et al.* [20] and Chong *et al.* [21] could experimentally, numerically, and theoretically show that under such conditions the droplet radius of long-chain alcohols dissolving in water shrinks as $R(t) \sim (\tau - t)^{4/5}$, leading to a droplet lifetime $\tau \sim R_0^{5/4}$.

However, the droplet dissolution process can induce not only body forces such as buoyancy, but also surface forces such as Marangoni forces [6,22,23]. For example, Tan *et al.* [24] showed that the solutal Marangoni flow at the interface of a binary water-ethanol droplet dissolving in anethole oil governs the drop dissolution process. Escobar *et al.* [25] observed a dramatically enhanced and temporally nonmonotonic droplet dissolution rate, which was triggered by solutal Marangoni flow, in the peculiar geometry of a water-immersed sessile long-chain alcohol droplet with an entrapped bubble.

Not only emerging concentration gradients can induce body or surface forces acting back on the droplet dissolution process itself, but also thermal gradients can do so. When the droplet is immersed in another liquid, a temperature gradient not only induces thermal Marangoni flow, but also changes the solubility and hence the saturation concentration of the host liquid. This leads to a complex dissolution dynamics of the droplet, which in this paper we want to explore under controlled conditions.

The system we pick is a sessile water droplet sitting on a gold nanoparticle decorated surface and immersed in water-saturated 1-butanol. Thanks to the plasmonic effect of the gold nanoparticles, the area under the droplet can locally be heated [26–28]: Upon irradiation with a continuous wave laser at the plasmonic resonance of the gold nanoparticles, a huge amount of thermal energy is locally deposited under the sessile droplet, leading to a strong temperature gradient. Under these conditions we experimentally find that the droplet dissolution time scales with the initial droplet radius as $\tau \sim R_0^4$. We then theoretically explain this new scaling behavior, based on an analysis of the thermal Marangoni forces, the thermal diffusion equation, and of the temperature dependent solubility of water in 1-butanol.

The paper is organized as follows: We briefly explain the experimental setup and the methods (Sec. II). We then report our experimental findings (Sec. III), which are explained in Sec. IV. The paper ends with conclusions and an outlook (Sec. V).

II. EXPERIMENTAL SETUP AND METHODS

In the experiment, the gold nanoparticle decorated substrate was placed in a quartz glass cuvette ($10 \times 10 \times 45$ mm) filled with a water–1-butanol mixture. Since the 1-butanol mixture was oversaturated with water, microsized water droplets nucleated on the substrate. We work in the limit of low sessile droplet area density so that no droplet-droplet interactions can occur. A continuous wave laser (Cobolt Samba) of 532 nm wavelength was used to irradiate the sample beneath the droplet from the bottom side. The laser power was controlled by using a half-wave plate and a polarizer and measured by a photodiode power sensor (S130C, ThorLabs). Two high-speed cameras were installed in the setup to monitor the dynamics of the dissolving droplet. One (Photron SA7) was equipped with a $5\times$ long working distance objective (LMPLFLN, Olympus) for bottom view imaging, and the other one (Photron SAZ) with a $10\times$ or $20\times$ long working distance objective and operated at 1 kfps for fast imaging. (For details in sample preparation and the experimental setup, please refer to our previous study in Ref. [28]).
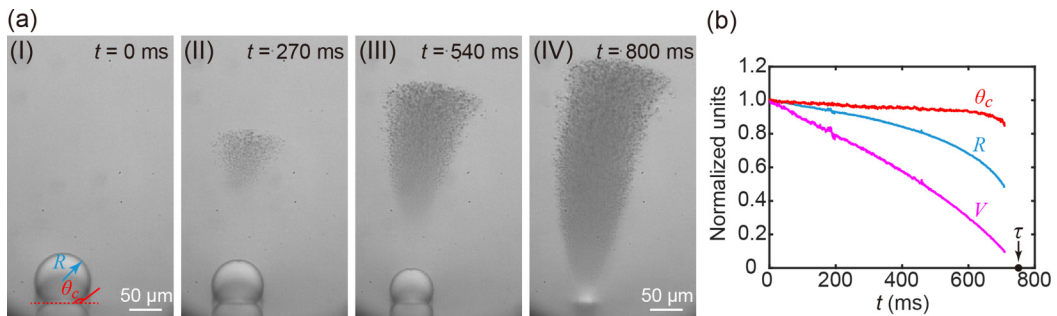
FIG. 1. (a) Snapshots of a dissolving water droplet in water-saturated 1-butanol at different instants of time under laser power $P_\ell = 40$ mW. (b) Evolution of volume V, radius R, and contact angle θ_c in time. All parameters have been normalized by their initial values: $V_0 = 0.32$ nL, $R_0 = 44$ μm, and $\theta_0 \approx 130°$, respectively.

III. EXPERIMENTAL RESULTS

Sequential snapshots of a typical dissolving water droplet in water-saturated 1-butanol solution under laser irradiation are shown in Fig. 1(a). Immediately after laser irradiation, the droplet starts to shrink [Fig. 1(a-I)]. At 270 ms, a plume appears and moves off wall away from the droplet [Fig. 1(a-II)]. With time, the plume grows [Fig. 1(a-III)] until the droplet is completely dissolved at 800 ms [Fig. 1(a-IV)]. Figure 1(b) displays the volume V, radius R, and contact angle θ_c of the droplet as a function of time t during the dissolution process. All values are normalized to their values at $t = 0$, which is the moment the laser was turned on. In the figure, τ refers to the moment when the droplet is completely dissolved; i.e., τ is the lifetime of the droplet. It is found that the contact angle θ_c of the droplet remains almost constant and only slightly decreases with time at the end of the dissolution process, which reflects dissolution in the constant contact angle mode [11]. The details of the whole dissolution process can be seen in Movie S1 of the Supplemental Material [29].

The dissolution of the water droplet is due to the increasing solubility of water in 1-butanol with increasing temperature [30]. As sketched in Fig. 2, the liquid around the droplet is heated up because of the plasmonic effect. The flow of water from the droplet into the 1-butanol solution implies a shrinkage of the water droplet. Besides the increased solubility of water in 1-butanol, the thermal Marangoni flow contributes to the droplet dissolution as well. The temperature of the droplet is highest at the bottom of the droplet and lowest at its top [31]. As the surface tension decreases with increasing temperature, the surface tension is highest at the top of the water droplet [32]. This causes an off-wall thermal Marangoni flow around the droplet interface [33], which can be confirmed by the flow field constructed through a particle image velocimetry (PIV) measurement inside the water droplet, as shown in Appendix A and Movie S2 [29]. The Marangoni flow brings the hot 1-butanol solution with a high water concentration c_w to the region above the droplet. In the region just above the droplet, the temperature of the mixture liquid is still very high and hence the solubility of water in 1-butanol is still high. With increasing height, however, the temperature of the liquid drops and the solubility decreases until eventually the 1-butanol becomes saturated and nucleation of tiny water droplets sets in. These then form a cloud or plume, as clearly seen in Figs. 1(a-II)–1(a-IV).

One wonders whether gravity effects also play a role. To find out, we estimate the Archimedes number (also called Grashof number), which compares the driving force due to gravity with the viscous force, $\text{Ar} = gR_\mu^3 \Delta\rho/(\rho_0\nu^2)$. The density difference $\Delta\rho$ between that of the (heavier) water ρ and the (lighter) water-saturated 1-butanol ρ_0 is 152 kg/m^3 and the kinematic viscosity of 1-butanol at room temperature $\nu \approx 4\times10^{-6}$ m^2/s. This implies that even a very large microdroplet
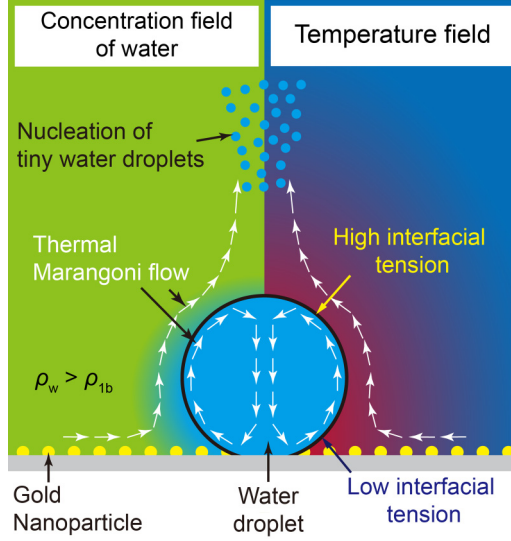
FIG. 2. Schematic diagram of the plume formation above a dissolving water droplet in the surrounding water-saturated 1-butanol. The plasmonic effect induced temperature field leads to an increased water solubility and a decreased surface tension of 1-butanol solution near the bottom of the water droplet. As a result, an off-wall thermal Marangoni flow is generated, transporting the hot 1-butanol solution with a high water concentration to the cold region above the droplet, leading to the nucleation of a water droplet plume. As explained in the main text, gravity does not play any role here; the flow is solely driven by thermal Marangoni forces.

of $R_\mu = 100\ \mu$m has an Archimedes number of Ar ≈ 0.1, so that gravity effects do not play a role. In addition, gravity effects would point downwards towards the sessile drop, as water is heavier than 1-butanol, but the plume of water microdroplets in Figs. 1(a-II)–1(a-IV) points upwards (here off wall), clearly ruling out gravitational effects. Note that the plasmonic heating on the liquid outside the water droplet can reduce the liquid density, and thus may lead to an upward flow as well. However, by referring to Movie S1 [29], it can be clearly seen that the upward flow above the droplet rapidly slows down when the droplet is almost dissolved, indicating that the buoyancy effect caused by the plasmonic heating is negligible comparing with the thermal Marangoni force.

To measure the fluid flow caused by the thermal Marangoni effect, we performed PIV measurements. Polystyrene particles (Thermo Scientific, Fluoro-Max Red) with a diameter of 5 μm and a concentration of 60 μg/mL were added to the water-saturated 1-butanol solution. The flow velocity profiles near the water droplet at $t = 1, 8$, and 15 s are shown in Fig. 3(a). The data clearly reveals that there is an off-wall flow. For details of the PIV measurements, we refer to Movie S3 in the Supplemental Material [29].

We extracted the flow velocities v at three selected regions [marked as 1, 2, and 3 in Fig. 3(a-I)] above the droplet. The results are shown in Fig. 3(b). For these three locations, the flow velocity v near the top of the droplet increases with increasing distance from the droplet. The dependence of the velocity of the polystyrene particles in the boxes outlined in Fig. 3(a) is shown in Fig. 3(b). Here we take the velocity v in the selected area marked by the green box as the Marangoni velocity v_M. As depicted by the green curve in Fig. 3(b), v_M increases from 5×10^{-5} to 5×10^{-4} m/s during the dissolution process when R decreases from 102 to 90 μm. After that, v_M gradually decreases to 3×10^{-4} m/s at a droplet radius of 45 μm.

The velocity of the thermal Marangoni convection is proportional to the surface tension gradient along the droplet interface, namely, $v_M \sim \Delta\sigma \approx 2R(\partial\sigma/\partial T)(\partial T/\partial y)$, where $\partial T/\partial y$ is the temperature gradient in vertical direction. Since the Péclet number (the ratio of thermal convection and
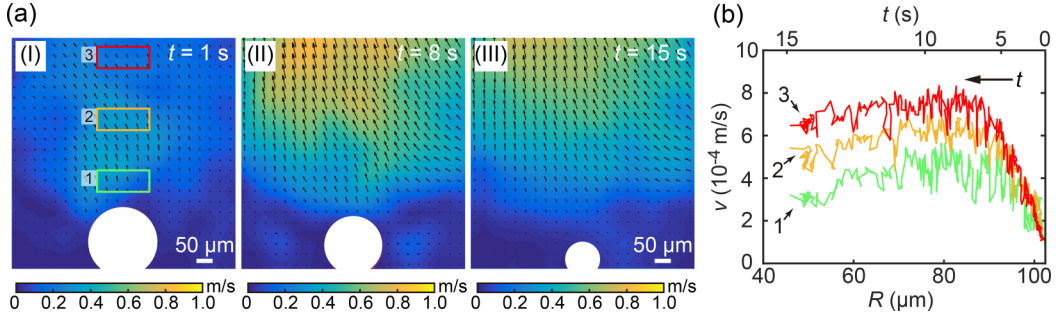
FIG. 3. (a) Particle image velocimetry of the liquid in the vicinity of a dissolving droplet at different instants of time at a laser power of $P_\ell = 40$ mW. (b) Measured mean liquid velocity as a function of the droplet radius (and thus time) as measured with PIV in the three selected regions 1, 2, and 3, as shown in panel (a-I).

thermal diffusion) Pe $\approx v_M R/\kappa < 0.4$, where $v_M \approx 5 \times 10^{-4}$ m/s is the maximum velocity extracted from Fig. 3(b) for the fluid flow in the green box shown in Fig. 3(a-I) and $\kappa = 7.6 \times 10^{-8}$ m^2/s is the thermal diffusivity coefficient in the water-saturated 1-butanol mixture, thermal diffusion plays a more dominant role in the droplet dissolution process than convection. Therefore the plasmonic induced temperature field can, at least after some time, be considered to be quasistationary. This quasistationary state of the temperature field can also be verified by comparing the characteristic time of the temperature field and the dissolution time of the droplet. Here the characteristic time of the temperature field is related to the thermal diffusion time τ_{diff}, which can be estimated by $\tau_{\text{diff}} \approx R^2/(\pi\kappa) \approx 11$ ms, where $R = 50$ μm is extracted from Fig. 1. One can see that τ_{diff} is much shorter than the droplet dissolution time $\tau = 800$ ms (see Fig. 1). Thus the steady state assumption of the temperature field is reasonable. Before this quasistationary stage, the temperature gradient $\partial T/\partial y$ rapidly increases, resulting in an increase of v_M. Subsequently, $\partial T/\partial y$ is stabilized, but the droplet shrinks continuously, leading eventually to a decrease of v_M.

To obtain a quantitative analysis of the droplet dissolution dynamics, we systematically conducted a series of experiments at different laser powers. Figure 4(a) shows the results of $R(t)$ versus $\tau - t$ for different droplets at different laser powers ranging from 20 to 60 mW. The volume loss rate (per area) $\dot{V}(t)/A(t)$ versus the droplet radius $R(t)$ is plotted in Fig. 4(b), where $A(t) \sim (R(t))^2$
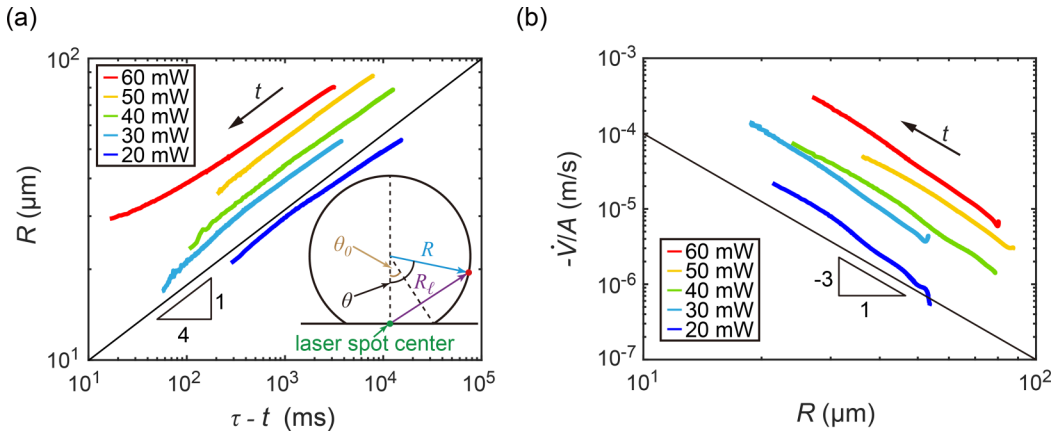

FIG. 4. (a) Droplet radius R as a function of $\tau - t$ on a double logarithmic scale. The solid black line refers to an exponent of 1/4. (b) Rate of volume loss per area $\dot{V}/A$ as a function of droplet radius R at different laser powers P_ℓ. The solid black line refers to the exponent -3.

is the surface area of the droplet. From the two plots, we find scaling laws close to

$$R(t) \sim (\tau - t)^{1/4} \tag{1}$$

and $\dot{V}/A \sim R^{-3}$, respectively and consistently.

Equation (1) is our main experimental result. We emphasize that this scaling law Eq. (1), which implies a droplet lifetime of $\tau \sim R_0^4$, is pronouncedly different from $R(t) \sim (\tau - t)^{1/2}$ as known for pure diffusive dissolution [11] and also from $R(t) \sim (\tau - t)^{4/5}$ known for natural convection dominated dissolution due to gravity effects [20,21]. In the next section we will set out to theoretically explain this scaling behavior.

IV. THEORETICAL EXPLANATION OF THE EXPERIMENTALLY FOUND DISSOLUTION BEHAVIOR

To explain this new scaling law, a simplified theoretical model is developed to describe the droplet dissolution process. The mass transfer rate of the droplet is proportional to the concentration gradient $\partial_r c_w|_R$ at the interface between the water droplet and the surrounding liquid, where r is the radial coordinate from the center of the droplet. The total mass loss rate $\dot{m}$ of the sessile droplet can be obtained by integrating over the water droplet,

$$\dot{m} = \rho \dot{V} = D \int_{\theta_0}^{\pi} 2\pi R^2 \sin\theta \, \partial_r c_w|_R d\theta, \tag{2}$$

where D is the mass diffusivity coefficient of water in 1-butanol, θ_0 is the angle shown in Fig. 4(a), θ is the angle between the droplet radius and the vertical line [θ_0 and θ are depicted in the inset figure in Fig. 4(a)], and R is the radius of the water droplet. Note that we assume that the water concentration c_w in 1-butanol at the droplet interface is always in equilibrium at its saturation concentration c_s, namely, $c_w = c_s$ at the droplet interface [20,21,34]. The water concentration gradient $\partial_r c_w|_R$ at the droplet interface is given by

$$\partial_r c_w|_R = \frac{\partial c_s}{\partial T} \partial_r T|_{R,b} = 2a(T - T_0) \partial_r T|_{R,b}, \tag{3}$$

where c_s is the saturation concentration of water in 1-butanol, $a = 0.0118 \text{ kg/(m}^3 \text{ K}^2)$ is a known material parameter (for details, we refer to Fig. 7 in Appendix B), T is the temperature, $T_0 = 20°C$ is the room temperature, and $\partial_r T|_{R,b}$ is the temperature gradient outside the droplet at the droplet interface. Note that the laser heating can be approximated as a point source, since most of the time the laser spot is smaller than the droplet size. In addition, as mentioned earlier, the temperature field can be taken as quasistationary, i.e., $\partial_t T = 0$, leading to the Laplace equation

$$\partial_t T(r_\ell, t) = \kappa \frac{1}{r_\ell^2} \partial_{r_\ell} \left(r_\ell^2 \partial_{r_\ell} T(r_\ell, t) \right) = 0, \tag{4}$$

where r_ℓ is the radial coordinate from the laser spot center and κ is the thermal diffusivity. By solving Eq. (4) at $r_\ell = R_\ell$, where R_ℓ is the distance between the droplet interface and the laser spot center [Fig. 4(a)], we obtain

$$\partial_{r_\ell} T|_{R_\ell, w} = -\frac{b}{R_\ell^2}, \quad T - T_0 = \frac{b}{R_\ell}, \tag{5}$$

where $\partial_{r_\ell} T|_{R_\ell, w}$ is the temperature gradient inside the water droplet at the droplet interface along the direction of R_ℓ, and b is a prefactor. With $\partial_{r_\ell} T|_{R_\ell, w}$, we can now obtain the normal component $\partial_r T|_{R, w}$ to the spherical droplet surface,

$$\partial_r T|_{R, w} = \partial_{r_\ell} T|_{R_\ell, w} \frac{\partial R_\ell}{\partial R} = \partial_{r_\ell} T|_{R_\ell, w} f(\theta), \tag{6}$$
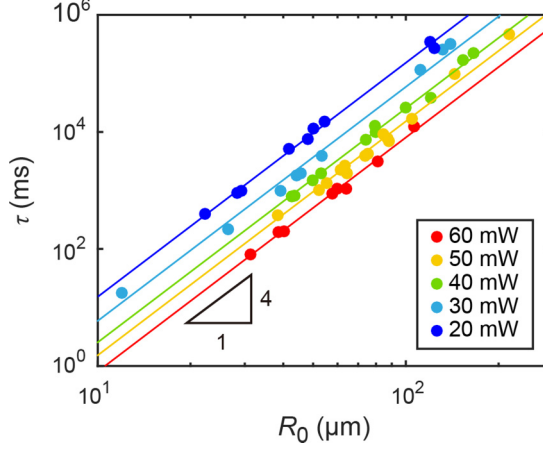
FIG. 5. Dissolution time τ of water droplets as a function of the initial droplet radius R_0 at different laser powers P_ℓ. The droplet lifetime τ obeys the scaling law of $\tau \sim R_0^4$. The solid lines are drawn to guide the eye.

where $f(\theta) = \sqrt{\sin^2 \theta + (\cos \theta_0 - \cos \theta)^2}$. Note that the temperature gradients inside the water droplet, $\partial_r T|_{R,w}$, and outside the droplet, $\partial_r T|_{R,b}$, at the droplet interface are not the same due to the different thermal conductivities of the water droplet and the surrounding liquid (water-saturated 1-butanol). Considering the conserved heat flux ϕ across the water droplet interface, we have the following relationship:

$$\phi = -k_w \, \partial_r T|_{R,w} = -k_b \, \partial_r T|_{R,b}, \tag{7}$$

where k_w and k_b are the thermal conductivities of water and water-saturated 1-butanol, respectively. By solving Eq. (7), we get

$$\partial_r T|_{R,b} = \frac{k_w}{k_b} \, \partial_r T|_{R,w}. \tag{8}$$

By substituting Eqs. (3), (5), (6), and (8) into Eq. (2), we obtain

$$\dot{V} = -\frac{4\pi a b^2 D k_w}{\rho k_b} \int_{\theta_0}^{\pi} \frac{\sin \theta}{f(\theta)^2} d\theta \frac{1}{R} \sim \frac{1}{R}. \tag{9}$$

Equation (9) can easily be integrated, resulting in $\dot{V}/A \sim R^{-3}$, and $R \sim (\tau - t)^{1/4}$. These results are consistent with our experimental results as seen from Figs. 4(b) and 4(a). We also obtain the dissolution time or lifetime τ of the droplet as

$$\tau = \frac{(2 - \cos \theta_0)(1 + \cos \theta_0)^2 \rho k_b}{16 a b^2 D k_w \int_{\theta_0}^{\pi} \frac{\sin \theta}{f(\theta)^2} d\theta} R_0^4 \sim R_0^4. \tag{10}$$

To obtain further evidence for our theoretical model, we measured the lifetime of water droplets with various initial radii R_0 varying in the large range of 10 to 200 μm at different laser powers P_ℓ. The results are summarized in Fig. 5. The agreement between the scaling law in Eq. (10) and the experimental results is excellent. This supports the validity of the proposed scaling for all considered laser powers and droplet sizes.

V. CONCLUSIONS AND OUTLOOK

In summary, we have experimentally and theoretically studied the dissolution of a water droplet in a water-saturated 1-butanol solution. The laser irradiation induced plasmonic heating of the liquid
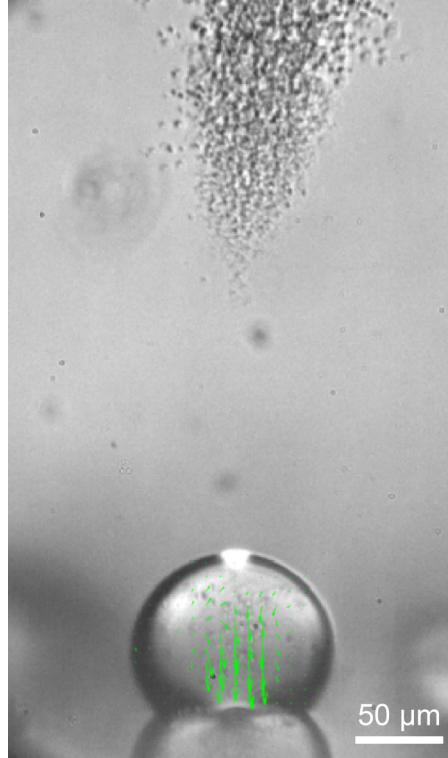
FIG. 6. Flow field inside the water droplet under plasmonic effect.

around the droplet results in (1) the uptake of water in the 1-butanol and (2) an off-wall thermal Marangoni flow. As a result, the hot 1-butanol solution with a relative high water concentration is transported to the cold region, where the water solubility is lower. This leads to the formation of a plume consisting of tiny water microdroplets. Most importantly, the thermal gradient and the thermal Marangoni flow around the droplet affect its dissolution dynamics and make it very different from isothermal and purely diffusive dissolution dynamics or the dissolution dynamics due to natural convection, which lead to droplet lifetimes of $\tau \sim R_0^2$ and $\tau \sim R_0^{5/4}$, respectively. In contrast, here we have experimentally found that the droplet lifetime scales as the fourth power of the initial droplet radius, $\tau \sim R_0^4$, and have provided a theoretical model to account for this new dissolution behavior.

We expect that nonstandard droplet or bubble dissolution laws can also hold in other situations where thermal or solutal Marangoni flows play a role, including those of relevance in applications, such as in catalysis or electrolysis, where bubbles can evolve at catalytic surfaces or on electrodes [35–38]. In these cases the bubbles are hindering the catalytic or electrolytic processes and an understanding of the effect of the Marangoni forces and the temperature dependent solubility may help to enhance the bubble dissolution. Another situation where Marangoni forces may affect the dissolution behavior are droplets driven by autochemotaxis [9,10,39–41].
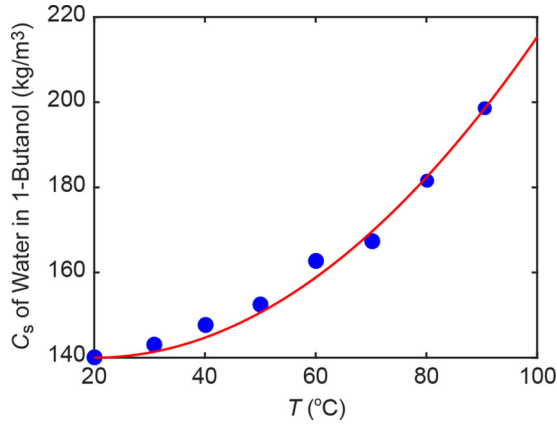
FIG. 7. The saturation concentration c_s of water in 1-butanol as a function of the temperature T. Data points are from Ref. [30]. The solid curve is the result of a least-squares quadratic fitting of the data points to Eq. (B1).

APPENDIX A: FLOW FIELD INSIDE THE WATER DROPLET

The flow field inside the water droplet under plasmonic effect is shown in Fig. 6, in which a strong downward flow in the center of the droplet is observed. This implies an upward thermal Marangoni flow at the droplet interface. For details, we refer to Movie S2 in the Supplemental Material [29]. The movie clearly shows that there is an upward flow around the droplet interface.

APPENDIX B: SOLUBILITY DEPENDENCE

The saturation concentration (solubility) c_s of water in 1-butanol as a function of temperature T is shown in Fig. 7. It is found that c_s can be well described by a quadratic function in the temperature T,

$$c_s - c_{s0} = a(T - T_0)^2, \tag{B1}$$

where c_{s0} is the saturation concentration of water in 1-butanol at room temperature, $T_0 = 20°C$, and $a = 0.0118 \text{ kg/(m}^3 \text{ K}^2)$ is a material constant. By taking the derivative of Eq. (B1) with respect to T, we obtain

$$\frac{\partial c_s}{\partial T} = 2a(T - T_0). \tag{B2}$$

[1] A. Gupta, H. B. Eral, T. A. Hatton, and P. S. Doyle, Nanoemulsions: Formation, properties and applications, Soft Matter **12**, 2826 (2016).

[2] W.-L. Chou, P.-Y. Lee, C.-L. Yang, W.-Y. Huang, and Y.-S. Lin, Recent advances in applications of droplet microfluidics, Micromachines **6**, 1249 (2015).

[3] L. Wang, J. Dong, J. Chen, J. Eastoe, and X. Li, Design and optimization of a new self-nanoemulsifying drug delivery system, J. Colloid Interface Sci. **330**, 443 (2009).

[4] A. Jain and K. K. Verma, Recent advances in applications of single-drop microextraction: A review, Anal. Chim. Acta **706**, 37 (2011).

[5] D. Lohse, Towards controlled liquid-liquid microextraction, J. Fluid Mech. **804**, 1 (2016).

[6] D. Lohse and X. Zhang, Physicochemical hydrodynamics of droplets out of equilibrium, Nat. Rev. Phys. **2**, 426 (2020).

[7] Z. Lu, A. Rezk, F. Jativa, L. Yeo, and X. Zhang, Dissolution dynamics of a suspension droplet in a binary solution for controlled nanoparticle assembly, Nanoscale **9**, 13441 (2017).

[8] E. Um, J. K. Nunes, T. Pico, and H. A. Stone, Multicompartment microfibers: Fabrication and selective dissolution of composite droplet-in-fiber structures, J. Mater. Chem. B **2**, 7866 (2014).

[9] C. Jin, C. Krüger, and C. C. Maass, Chemotaxis and autochemotaxis of self-propelling droplet swimmers, Proc. Natl. Acad. Sci. USA **114**, 5089 (2017).

[10] B. Liebchen and H. Löwen, Synthetic chemotaxis and collective behavior in active matter, Acc. Chem. Res. **51**, 2982 (2018).

[11] D. Lohse and X. Zhang, Surface nanobubble and surface nanodroplets, Rev. Mod. Phys. **87**, 981 (2015).

[12] A. M. Cazabat and G. Guéna, Evaporation of macroscopic sessile droplets, Soft Matter **6**, 2591 (2010).

[13] H. Y. Erbil, Evaporation of pure liquid sessile and spherical suspended drops: A review, Adv. Colloid Interface Sci. **170**, 67 (2012).

[14] I. Langmuir, The evaporation of small spheres, Phys. Rev. **12**, 368 (1918).

[15] P. S. Epstein and M. S. Plesset, On the stability of gas bubbles in liquid-gas solutions, J. Chem. Phys. **18**, 1505 (1950).

[16] R. D. Deegan, O. Bakajin, T. F. Dupont, G. Huber, S. R. Nagel, and T. A. Witten, Capillary flow as the cause of ring stains from dried liquid drops, Nature (London) **389**, 827 (1997).

[17] Y. O. Popov, Evaporative deposition patterns: Spatial dimensions of the deposit, Phys. Rev. E **71**, 036313 (2005).

[18] W. F. Wells, On air-borne infection: Study II. Droplets and droplet nuclei, Am. J. Epidemiol. **20**, 611 (1934).

[19] O. R. Enríquez, C. Sun, D. Lohse, A. Prosperetti, and D. van der Meer, The quasi-static growth of CO_2 bubbles, J. Fluid Mech. **741**, R1 (2014).

[20] E. Dietrich, S. Wildeman, C. W. Visser, K. Hofhuis, E. S. Kooij, H. J. W. Zandvliet, and D. Lohse, Role of natural convection in the dissolution of sessile droplets, J. Fluid Mech. **794**, 45 (2016).

[21] K. L. Chong, Y. Li, C. S. Ng, R. Verzicco, and D. Lohse, Convection-dominated dissolution for single and multiple immersed sessile droplets, J. Fluid Mech. **892**, A21 (2020).

[22] L. Scriven and C. Sternling, The Marangoni effects, Nature (London) **187**, 186 (1960).

[23] A. De Wit, Chemo-hydrodynamic patterns and instabilities, Annu. Rev. Fluid Mech. **52**, 531 (2020).

[24] H. Tan, C. Diddens, A. A. Mohammed, J. Li, M. Versluis, X. Zhang, and D. Lohse, Microdroplet nucleation by dissolution of a multicomponent drop in a host liquid, J. Fluid Mech. **870**, 217 (2019).

[25] J. M. Encarnación Escobar, J. Nieland, A. van Houselt, X. Zhang, and D. Lohse, Marangoni puffs: Dramatically enhanced dissolution of droplets with an entrapped bubble, Soft Matter **16**, 4520 (2020).

[26] G. Baffou and R. Quidant, Thermo-plasmonics: Using metallic nanostructures as nano-sources of heat, Laser Photon. Rev. **7**, 171 (2013).

[27] G. Baffou, J. Polleux, H. Rigneault, and S. Monneret, Super-heating and micro-bubble generation around plasmonic nanoparticles under cw illumination, J. Phys. Chem. C **118**, 4890 (2014).

[28] Y. Wang, M. E. Zaytsev, G. Lajoinie, H. L. The, J. C. T. Eijkel, A. van den Berg, B. M. Weckhuysen, X. Zhang, H. J. W. Zandvliet, and D. Lohse, Giant and explosive plasmonic bubbles by delayed nucleation, Proc. Natl. Acad. Sci. USA **115**, 7676 (2018).

[29] See Supplemental Material at http://link.aps.org/supplemental/10.1103/PhysRevFluids.7.064006 for movies of water droplet dissolution under plasmonic effect and the flow field inside and outside the droplet.

[30] R. Stephenson and J. Stuart, Mutual binary solubilities: Water-alcohols and water-esters, J. Chem. Eng. Data **31**, 56 (1986).

[31] B. Zeng, Y. Wang, M. E. Zaytsev, C. Xia, H. J. W. Zandvliet, and D. Lohse, Giant plasmonic bubbles nucleation under different ambient pressures, Phys. Rev. E **102**, 063109 (2020).

[32] S. Sugden, The variation of surface tension with temperature and some related functions, J. Chem. Soc. Trans. **125**, 32 (1924).

[33] B. Zeng, K. L. Chong, Y. Wang, C. Diddens, X. Li, M. Detert, H. J. W. Zandvliet, and D. Lohse, Periodic bouncing of a plasmonic bubble in a binary liquid by competing solutal and thermal Marangoni forces, Proc. Natl. Acad. Sci. USA **118**, e2103215118 (2021).

[34] Y. Wang, M. E. Zaytsev, H. L. The, J. C. T. Eijkel, H. J. W. Zandvliet, X. Zhang, and D. Lohse, Vapor and gas-bubble growth dynamics around laser-irradiated, water-immersed plasmonic nanoparticles, ACS Nano **11**, 2045 (2017).

[35] X. Yang, F. Karnbach, M. Uhlemann, S. Odenbach, and K. Eckert, Dynamics of single hydrogen bubbles at a platinum microelectrode, Langmuir **31**, 8184 (2015).

[36] A. Bashkatov, S. S. Hossain, X. Yang, G. Mutschke, and K. Eckert, Oscillating Hydrogen Bubbles at Pt Microelectrodes, Phys. Rev. Lett. **123**, 214503 (2019).

[37] X. Yang, D. Baczyzmalski, C. Cierpka, G. Mutschke, and K. Eckert, Marangoni convection at electrogenerated hydrogen bubbles, Phys. Chem. Chem. Phys. **20**, 11542 (2018).

[38] D. Lohse, Bubble puzzles: From fundamentals to applications, Phys. Rev. Fluids **3**, 110504 (2018).

[39] S. Bekki, M. Vignes-Adler, and E. Nakache, Solutal Marangoni effect: II. Dissolution, J. Colloid Interface Sci. **152**, 314 (1992).

[40] Y.-J. Chen, Y. Nagamine, and K. Yoshikawa, Self-propelled motion of a droplet induced by Marangoni-driven spreading, Phys. Rev. E **80**, 016303 (2009).

[41] B. V. Hokmabad, R. Dey, M. Jalaal, D. Mohanty, M. Almukambetova, K. A. Baldwin, D. Lohse, and C. C. Maass, Emergence of Bimodal Motility in Active Droplets, Phys. Rev. X **11**, 011043 (2021).